New results in stellarator optimisation

M. Drevlak , C. D. Beidler, J. Geiger, P. Helander, S. Henneberg, C. Nührenberg, Y. Turkin
Max-Planck-Institut für Plasmaphysik, 17491 Greifswald, Germany
Email: drevlak@ipp.mpg.de

Abstract

The ROSE code was written for the optimisation of stellarator equilibria. It uses VMEC for the equilibrium calculation and several different optimising algorithms for adjusting the boundary coefficients of the plasma. Some of the most important capabilities include optimisation for simple coils, the ability to simultaneously optimise vacuum and finite beta field, direct analysis of particle drift orbits and direct shaping of the magnetic field structure. ROSE was used to optimise quasi-isodynamic, quasi-axially symmetric and quasi-helically symmetric stellarator configurations.

1. Introduction

The performance of stellarators, characterised by properties related to MHD stability, confinement of fast particles, neoclassical and anomalous transport and engineering complexity, is known to depend strongly on the underlying equilibrium configuration. While the first fully optimised stellarators, HSX and Wendelstein 7-X, have entered operation, new stellarator designs are being considered. In particular, a possible stellarator reactor needs to be optimised beyond the optimisation level achieved for these devices. A strong need for progress has been identified in the confinement of fast particles significantly away from the magnetic axis. At the same time, coil complexity must not exceed the limits of feasibility.

2. The ROSE Code

The ROSE [1] code was written for the optimisation of stellarator equilibria. Like other tools created for the optimisation of stellarator equilibria [2] [3], it uses VMEC [4] for the equilibrium calculation and several different optimising algorithms for adjusting the coefficients of the boundary shape of the plasma. The procedural structure of ROSE is outlined in Fig. 1. The code is written in C++ and allows, at the time of this writing, parallel execution of the external codes (VMEC...) when feasible.

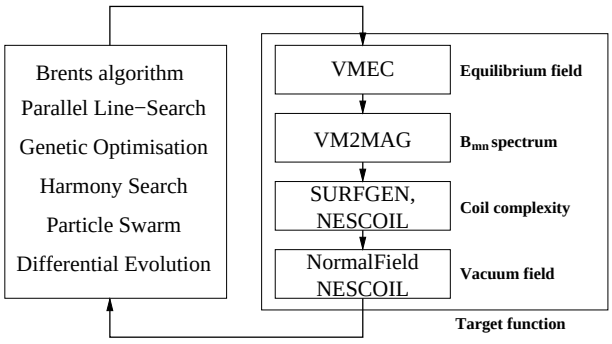

Figure 1: Procedural structure of the ROSE code.

The scope of properties the code can target includes geometrical properties of the plasma boundary, deviation from quasi-symmetries, neoclassical transport, the rotational transform profile, magnetic mirror ratios, and many others. In addition to these criteria, which are relatively common in previous designs, the code has been extended to include optimisation targets that are new to stellarator optimisation. These include an analysis of the vacuum magnetic field and a new way to assess coil complexity.

A more comprehensive overview of the criteria available for the target function optimised is given below.

- gaussian curvature on plasma boundary
- maximum absolute value among the principal curvatures: $\sup\{|K_1|, |K_2|\}$
- aspect ratio (unless fixed a priori)
- rotational transform ι at selected radial positions s
- regions with undesired sign of shear
- magnetic well at design $\langle\beta\rangle$
- field ripple on magnetic axis $\mathcal{R} = \frac{B_{max}-B_{min}}{B_{max}+B_{min}}$
- magnetic mirror at flux surface s $\mathcal{M} = \frac{B(s,u=0,v=0)-B(s,u=0,v=1/2)}{B(s,u=0,v=0)+B(s,u=0,v=1/2)}$
- deviation of the B_{mn} from quasi-symmetry
- ratios between arbitrary B_{mn} components
- ϵ_{eff} on arbitrary field lines [29]
- radial drift velocity parameters Γ_v, Γ_w, Γ_c [30] as indicators of fast α-particle confinement
- var(B) on the contours of maximum and minimum B at the toroidal symmetry planes
- var(J) at flux surface
- properties involving the vacuum field
  - vacuum rotational transform on the axis
  - vacuum magnetic well
  - Shafranov shift
- properties related to coil complexity
- proxy for turbulent transport [5]
- drift orbits [31]
- mercier stability computed by VMEC
- MHD stability evaluated with CAS3D

2.1. Vacuum Field Analysis

For many configuration properties, it is desirable to carry out the optimisation at finite plasma pressure. This is particularly the case for qualities related to fast-particle confinement, the accuracy of quasi-symmetries, or the effective ripple. These properties depend on the plasma pressure, and it is their value at finite $\langle\beta\rangle$ that is decisive for the performance of the stellarator in question. However, important properties of the vacuum field can become difficult to discern or assume unfavourable values. For instance, due to the diamagnetic property of the plasma, the magnetic well can be positive [corresponding to negative $V''(s)$] at finite $\langle\beta\rangle$ but turn into a magnetic hill ($\mathcal{V}'' > 0$) when the vacuum field is analysed.

Analyses of vacuum field properties have been done before in the scope of the NCSX design effort [6]. There, the vacuum field was evaluated using a virtual casing (VC) directly on the plasma boundary.

The approach implemented for ROSE proceeds along three major steps:

1. calculate the normal magnetic field from plasma currents on the plasma boundary
2. compute a current sheet generating the true vacuum field using SURFGEN and NESCOIL
3. evaluate vacuum field properties using the vacuum field computed from the current sheet using the Biot-Savart formula

The details of these steps will be outlined in the following sections.

2.1.1. Calculating the normal magnetic field

The virtual-casing principle is used to obtain the normal field from plasma currents exactly on the plasma boundary. Then, the field in the entire plasma domain is obtained by a NESCOIL calculation corrected for the normal field on the plasma boundary.

To explain this procedure in greater detail, let us divide $\mathbb{R}^3$ into 2 disjoint domains V_1 and V_2, with current distributions $\mathbf{J}_1$ and $\mathbf{J}_2$ in each of these. The current densities $\mathbf{J}_1$ and $\mathbf{J}_2$ generate contributions $\mathbf{B}_1$ and $\mathbf{B}_2$ to the magnetic field so that $\mathbf{B}_1(x) + \mathbf{B}_2(x) = \mathbf{B}(x)$ Assume, finally, that the boundary δV between V_1 and V_2 is located so that $\mathbf{B} \cdot \mathbf{n} = 0$.

If V_1, V_2 are chosen as the domains inside and outside the plasma boundary, then $\mathbf{B}_1$ and $\mathbf{B}_2$ are the magnetic field contributions from inner and outer currents respectively. $\mathbf{B}\cdot\mathbf{n}=0$ on the plasma boundary implies that $\mathbf{B}_1\cdot\mathbf{n}$ and $\mathbf{B}_2\cdot\mathbf{n}$ have the same magnitude.

In the following, let $\mathbf{p}(u,v)$ or $\tilde{\mathbf{p}}(u,v)$ denote points on the boundary surface and $\mathbf{p}_u=\frac{\mathrm{d}\mathbf{p}}{\mathrm{d}u}$, $\mathbf{p}_v=\frac{\mathrm{d}\mathbf{p}}{\mathrm{d}v}$, so that $\mathbf{n}=\frac{(\mathbf{p}_u\times\mathbf{p}_v)}{\|\mathbf{p}_u\times\mathbf{p}_v\|}$ denotes the normalised normal vector. The virtual-casing principle [7] as stated by Shafranov and Zakharov states that a mirror current density on δV defined by

$$\mathbf{J}_{mirror}(\mathbf{p})=-\mathbf{B}(\mathbf{p})\times\mathbf{n}(\mathbf{p}) \tag{1}$$

creates a magnetic field,

$$\mathbf{B}_{mirror}(\mathbf{x})=\frac{\mu_0}{4\pi}\int_{\delta V}\frac{\mathbf{J}(\tilde{\mathbf{p}})\times(\mathbf{x}-\tilde{\mathbf{p}})}{\|\mathbf{x}-\tilde{\mathbf{p}}\|^3}\mathrm{d}\mathbf{A}, \tag{2}$$

such that

$$\mathbf{B}_{mirror}(\mathbf{x})=\begin{cases}\mathbf{B}_2(\mathbf{x}) & \mathbf{x}\in V_1\\ -\mathbf{B}_1(\mathbf{x}) & \mathbf{x}\in V_2\end{cases} \tag{3}$$

For a mathematically rigorous treatment of the virtual-casing principle the reader is encouraged to consult Ref. [8].

The evaluation of equation (2) needs to deal with a singularity in the Biot-Savart rule and requires a little sleight of hand. A similar calculation has been implemented in the BNORM code by Merkel [9]. The calculation starts by seeking the Biot-Savart integral for the vector potential:

$$\mathbf{A}_{mirror}(\mathbf{p})=\frac{\mu_0}{4\pi}\int_0^{N_p}\int_0^1\frac{\mathbf{J}_{mirror}(\tilde{\mathbf{p}})\,\|\tilde{\mathbf{p}}_u\times\tilde{\mathbf{p}}_v\|}{\|\mathbf{p}-\tilde{\mathbf{p}}\|}\mathrm{d}u\mathrm{d}v$$

An explicit encounter with the singularity is avoided by computing $\mathbf{A}_{mirror}(p)$ on integer points $\mathbf{p}(i/N_u, N_pj/N_v)$ (N_u, N_v denoting the number of field lines, N_p the number of periods) using an open Newton-Cotes formula evaluating the integrand at half-integer points $\tilde{\mathbf{p}}((i+\frac{1}{2})/N_u, N_p(j+\frac{1}{2})/N_v)$.

In addition to using the dual mesh, the numerical integration is simplified (and hence accelerated) by eliminating the singular part from the integrand. This is achieved by writing

$$\begin{aligned}\mathbf{A}_{mirror}(\mathbf{p})=\frac{\mu_0}{4\pi}\int_{v-N_p/2}^{v+N_p/2}\int_{u-1/2}^{u+1/2}\Bigg[&\frac{\mathbf{J}_{mirror}(\tilde{\mathbf{p}})\,\|\tilde{\mathbf{p}}_u\times\tilde{\mathbf{p}}_v\|}{\|\mathbf{p}-\tilde{\mathbf{p}}\|}\\ &-\frac{\mathbf{J}_{mirror}(\mathbf{p})\,\|\mathbf{p}_u\times\mathbf{p}_v\|}{\sqrt{\hat{u}^2\mathbf{p}_u^2(u,v)+2\hat{u}\hat{v}\mathbf{p}_u(u,v)\mathbf{p}_v(u,v)+\hat{v}^2\mathbf{p}_v^2(u,v)}}\Bigg]\mathrm{d}\tilde{u}\mathrm{d}\tilde{v}\\ +\frac{\mu_0}{4\pi}\int_{v-N_p/2}^{v+N_p/2}\int_{u-1/2}^{u+1/2}&\frac{\mathbf{J}_{mirror}(\mathbf{p})\,\|\mathbf{p}_u\times\mathbf{p}_v\|}{\sqrt{\hat{u}^2\mathbf{p}_u^2(u,v)+2\hat{u}\hat{v}\mathbf{p}_u(u,v)\mathbf{p}_v(u,v)+\hat{v}^2\mathbf{p}_v^2(u,v)}}\mathrm{d}\tilde{u}\mathrm{d}\tilde{v}\end{aligned} \tag{4}$$

with $\hat{u}=\tilde{u}-u$, $\hat{v}=\tilde{v}-v$

The first of these integrals has the singularity removed and yields directly to numerical integration. Due to the interlaced meshes, an open Newton-Cotes formula is used. The second part of (4) can be integrated analytically in one of the coordinates.

The resulting 1d integral still has a singularity that is solved along the same lines as the first integration step. The singular part is treated by adding and subtracting a term with the same singularity. This results in a 1d integral without singularity, solved with an adaptive Gauss-Kronrod rule, and a second 1d integral, the integrand singular, that solves analytically.

After $\mathbf{A}_{mirror}$ has been computed on the integer mesh on the plasma boundary, the tangential components are interpolated using a 2d spline with periodic boundary conditions. The normal component $\mathbf{n} \cdot \mathbf{B}_{plasma}$ is then obtained by taking the normal component of **curl** $\mathbf{A}_{mirror}$. Since only the normal component of the magnetic field is needed, only the tangential derivatives of the tangential components of $\mathbf{A}_{mirror}$ are required.

Once the normal magnetic field from the plasma currents on the plasma boundary is available, a NESCOIL run is performed that is corrected for the normal magnetic field [10] [11] [12]. Unlike the NESCOIL calculation used to assess the coil complexity the current sheet for the vacuum field is not located in a region where the coils are expected, but in a region that is favourable for a benign NESCOIL solution and an efficient and accurate calculation of the Biot-Savart law. This is usually significantly closer to the plasma boundary than the coil set is.

2.2. Analysis of Coil Complexity

Coil complexity is an issue with the potential of deciding the technological feasibility of a stellarator configuration. Much effort has been made to address this difficulty. Coil optimisation tools like ONSET [16], COILOPT [13], FOCUS [14] or REGCOIL [15] are able to seek coil sets with optimised curvature radii and filament clearances. However, the optimisation of these properties may impair other properties of the resulting magnetic field. Boozer and Ku have proposed methods to include the response of relevant plasma properties to slight modifications of the configuration in order to extend the potential for easing coil construction in directions that do not compromise plasma performance [17] [18] [19].

Since there is an obvious competition between coil simplicity and other key parameters of the resulting configuration, ROSE takes takes the approach of striking this balance already at the design of the equilibrium. This can be achieved without actually having to design the coils simultaneously with the MHD equilibrium, but by adding adequate indicators for coil complexity to the equilibrium target function.

A good "guess" for coil complexity can be obtained from NESCOIL by computing the current sheet on a current-carrying surface (CCS) located roughly where the coils in the final machine would be. In a power plant, sufficient space between coils and plasma must be provided to accommodate a breeding blanket and neutron shielding. In practice, this imposes a limit on the minimum clearance between coils and plasma exceeding one metre.

The resulting approach to assessing coil complexity, repeated at each evaluation of a potential MHD equilibrium, proceeds along the following steps:

1. Use SURFGEN to generate a suitable current-carrying surface. This surface should have a shape resembling that of the plasma boundary and be situated at roughly constant distance from it.
2. Use NESCOIL to compute the current distribution J_c on the current surface.
3. Assess the complexity of this current distribution by evaluating the following properties:
   - Harmonic content of the current potential $\Phi = c_u u + c_v v + \sum_{k,l} s_{kl} \sin\left(2\pi\left(ku + lv\right)\right)$
     $\mathcal{H} = \sqrt{\frac{\sum_{k,l} s_{kl}^2 (k^2+l^2)}{c_u^2+c_v^2}}$,
   - Current compression: $\mathcal{C} = \frac{\max(J_c)-\min(J_c)}{\max(J_c)+\min(J_c)}$,
   - Geodesic and 3d curvature. The geodesic and 3d curvature, κ_g and κ,
   - Current islands. In a modular coil set, all current lines of the current sheet should close poloidally. However, the current potential may exhibit local extrema which lead to current

lines that close locally around the respective extremum instead of poloidally. Converted into actual coils, these current islands would correspond into saddle coils.

Current islands are detected by seeking locations where the gradient $\nabla_{u,v}\Phi(u,v)$ of the current potential becomes opposite to the regular gradient established by the total external current.

$$\mathcal{I} = \frac{1}{c_u^2 + c_v^2} \int\int T\left(-\left(\nabla_{u,v}\Phi(u,v) \cdot \begin{pmatrix} c_u \\ c_v \end{pmatrix} \right) + \gamma_t \right) \mathrm{d}u\mathrm{d}v \tag{5}$$

$$T(x) = \begin{cases} 0 & x < 0 \\ x & else \end{cases} \tag{6}$$

The parameter γ_t is a threshold parameter that facilitates detection and suppression of marginal current islands.

3. Optimisation Examples

The ROSE code was used to obtain optimised equilibria for several device classes holding the promise of adequate fast-particle confinement.

3.1. Quasi-isodynamic equilibrium

Quasi-isodynamic stellarators [22] are currently being explored with W7-X [23], [20]. These configurations hold the promise of combining sufficient fast-particle confinement and neoclassical transport with a small bootstrap currrent. This small current in turn allows the utilisation of an island divertor.

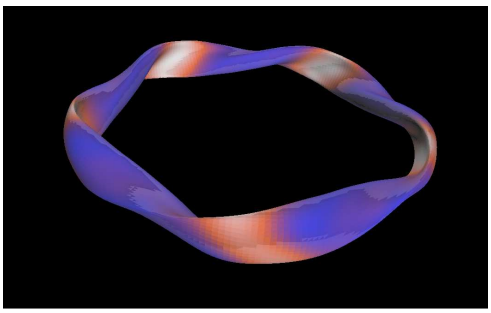

Figure 2: Optimised plasma boundary of a QI configuration at $A = 12.2$. The magnetic field strength is color coded.

The equilibrium presented here has $N_P = 5$ periods and an aspect ratio of $A = 12.2$. It exhibits enhanced fast-ion confinement off the magnetic axis compared with W7-X. It has a positive vacuum magnetic well and uses a similar range for the rotational transform with $\iota < 1$. The coil complexity is increased compared with W7-X.

3.2. Quasi-Axially Symmetric Equilibrium

In quasi-axially symmetric configurations [25] [26] the field strength exhibits a toroidal symmetry in Boozer coordinates. These devices are receiving worldwide attention as they could combine the advantages of stellarators and tokamaks. A reduced need for external rotational transform could lead to a simplified coil design. Nevertheless, this reduced external ι could be sufficient to ensure the existence of vacuum magnetic flux surfaces and prevent disruptions.

The equilibrium presented here [27] could lead to a medium-sized experiment to explore the potential of quasi-axisymmetry. It has an aspect ratio of $A = 3.4$, $N_P = 2$ and an external rotational transform of $\iota \sim 0.3$. This value was chosen in order to guarantee stability. The optimisation was carried out at a normalised plasma pressure of $\langle\beta\rangle = 0.035$. The accuracy of QA symmetry has been optimised to a qa-error of 0.28% at $s = 0.4$. The vacuum magnetic well is $\sim 3\%$. The quality of fast-particle confinement has been addressed through optimisation of the qa-error only.

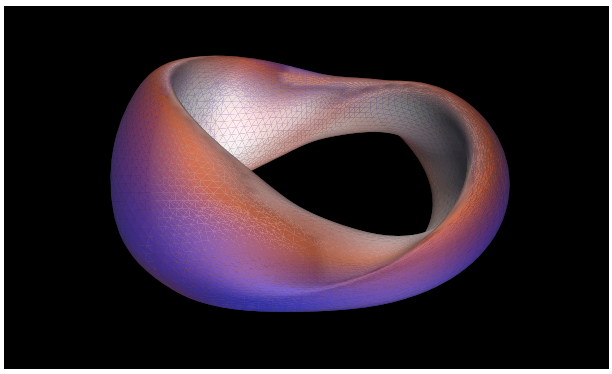

Figure 3: Plasma boundary of a quasi-axially symmetric stellarator with the magnetic field strength colour coded.

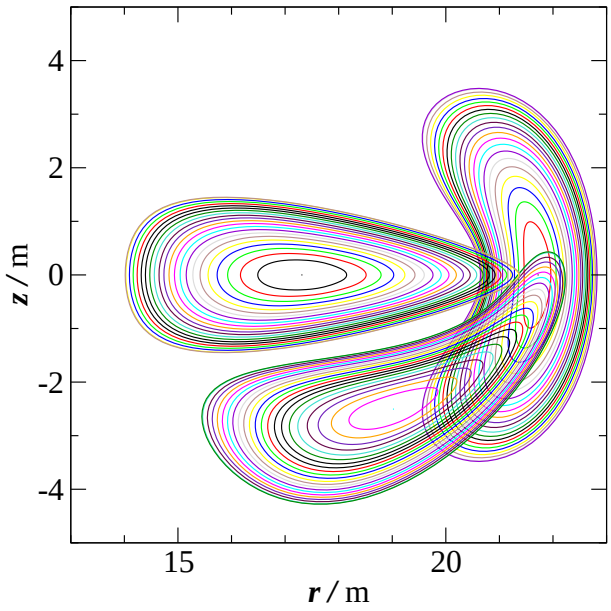

Figure 4: Cuts of the the flux surfaces of a quasi-helically symmetric configuration at selected toroidal angles.

3.3. Quasi-Helically Symmetric Equilibrium

Quasi-helically symmetric stellarators [24] [21] exhibit very good confinement and transport properties once a solution sufficiently close to ideal quasi-symmetry has been found. On the downside, the bootstrap current may be high. In contrast to other configurations, the bootstrap current in QH equilibria tends to reduce the rotational transform. As a result, no stable island structure will be available at the plasma edge and a divertor concept other than the island divertor needs to be employed.

The QH equilibrium presented here has an aspect ration of $A = 8.7$. Fig.4 shows selected cross-sections of the equilibrium. It clearly exhibits the large helical excursion of the magnetic axis typical of QH configurations. The qh-error, defined as the ratio between undesired modes and the average field, is 1.9% at $s = 1$. Improved confinement of fast particles will necessitate a further reduction of this value. An analysis of the structure of the magnetic field reveals that the variance of B on the minimal contour amounts to $\mathrm{var}(|B|) \sim 1.7\%$.

The optimisation was carried out at an elevated resolution. It used $N_{pol} = N_{tor} = 12$ Fourier modes in each angular direction and $N_s = 128$ radial flux surfaces. Regular optimisation typically uses $N_{pol} = N_{tor} \sim 6$ and $N_s \sim 60$. This high resolution allowed using the Mercier data generated by

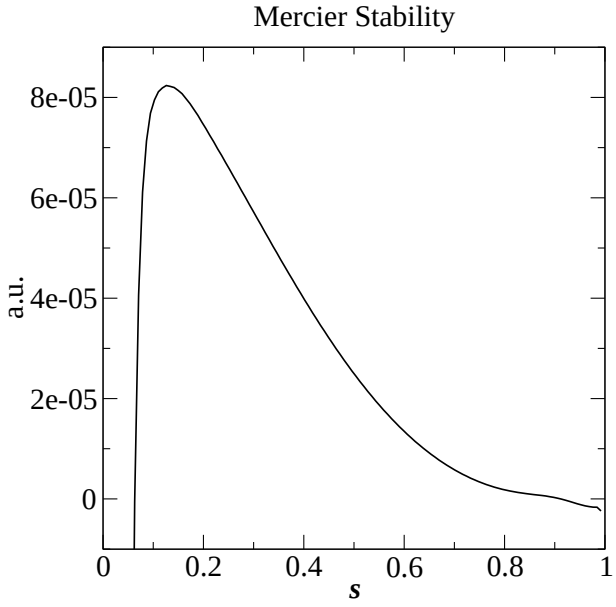

Figure 5: Mercier plot from VMEC data for a qh-symmetric configuration. Positive values indicate stability.

VMEC for an assessment of MHD stability. Fig. 5 indicates that the configuration is stable in the entire confinement domain.

Acknowledgements

The authors want to thank M. Borchardt, B. Kemnitz, A. Kleiber, A. Könies, J. Nührenberg and J. Riemann for discussions and support.

The work was supported in part by the Swiss National Science Foundation and by the Spanish Government (project ENE2014-52174-P) within the framework of the EUROfusion Consortium and received funding from the Euratom research and training programme 20142018 under grant agreement No 633053. The views and opinions expressed herein do not necessarily reflect those of the European Commission.

References

[1] M. Drevlak et al., *"Quasi-Isodynamic Configuration with Improved Confinement"*, 41st EPS Conference on Plasma Physics, Berlin, June 23 - 27, 2014

[2] D. A. Spong et al., *"Physics issues of compact drift optimized stellarators"* Nucl. Fusion **41** (2001) 711

[3] F. Castejon et al., *"Stellarator optimization under several criteria using metaheuristics"*, Plasma Phys. Control. Fusion **55** (2013) 014003

[4] S.P.Hirshman, van Rij, P.Merkel, *"Three-dimensional free boundary calculations using a spectral Greens function method"* Comput. Phys. Commun. **43**, 143 (1986)

[5] P. Xanthopoulos, private communication

[6] NCSX team, *private communication*

[7] V.D. Shafranov, L. E. Zakharov, *"Use of the virtual casing principle in calculating the containing magnetic field in toroidal plasma systems"* Nucl. Fusion **12** (1972) pp. 599

[8] J. D. Hanson, *"The virtual casing principle and Helmholtz's theorem"* Plasma Phys. Control. Fusion **57** (2015) 115006

[9] P. Merkel, *private communication*

[10] P. Merkel, M. Drevlak *"Coils for 3d MHD equilibria"* 1998 International Congress on Plasma Physics & 25th EPS Conference on Controlled Fusion and Plasma Physics, Praha, June 29 - July 3, 1998, Ed. P. Pavlo, pp. 1745

[11] P. Merkel, *"Solution of stellarator boundary value problems with external currents"* Nucl. Fusion **27** No. 5 (1987) pp.867

[12] P. Merkel, *"Applications of the Neumann problem to stellarators: Magnetic Surfaces, coils, free-boundary equilibrium, magnetic diagnostics"* Theory of Fusion Plasmas, Workshop Proceedings, Varenna, Italy, Aug. 24-28 1987 (pp. 25-46)

[13] D. J. Strickler, L. A. Berry, S. P. Hirshman, *"Designing coils for compact stellarators"* Fusion Science and Technology **41** No. 3 (2002) pp. 107

[14] Caoxiang Zhu et al., *"New method to design stellarator coils without the winding surface"* Nucl. Fusion **58** (2018) 016008

[15] M. Landreman *"An improved current potential method for fast computation of stellarator coil shapes"* Nucl. Fusion **57** (2017) 046003

[16] M. Drevlak, *"Coil Designs for a Quasi-Axially Symmetric Stellarator"*, 20th Symposium on Fusion Technology (1998), Marseille, pp. 883

[17] A. H. Boozer, *"Optimization of the current potential for stellarator coils"*, Phys. Plasmas Vol. **7** No. 2 (2000), pp. 629

[18] L.-P. Ku, A. H. Boozer, *"Stellarator coil design and plasma sensitivity"*, Phys. Plasmas **17** (2010) 122503

[19] A. H. Boozer *"Stellarator Design"* J. Plasma Phys. (2015), Vol. **81**, 515810606

[20] J.Nührenberg, R. Zille *"Stable stellarators with medium β and aspect ratio"* Physics Letters A, Volume 114A, No. 3 (1986) pp. 129

[21] A. F. Almagri et al., *"Design and construction of HSX: a helically symmetric stellarator"*, J. Plasma Fusion Res. SERIES, Vol.1 (1998) 422-425

[22] S. Gori, W. Lotz, J. Nührenberg, *"Quasi-isodynamic stellarators"*, Theory of Fusion Plasmas, Varenna 1996, pp. 335, Bologna, 1996, SIF.

[23] W. Lotz, J. Nührenberg, C. Schwab, *"Optimization, MHD Mode and Alpha Particle Confinement Behaviour of Helias Equilibria"*, Plasma Physics and Controlled Nuclear Fusion Research 1990, Nucl. Fusion Suppl., **(2)** pp. 603

[24] C. Nührenberg, M. I. Mikhailov, J. Nührenberg, V. D. Shafranov, **"Quasi-helical symmetry at finite aspect ratio"**, Plasma Physics Reports **36** No. 7, 558-562 (2010), DOI: 10.1134/S1063780X10070032, ISSN: 1063-780X (print) 1562-6938

[25] K. Matsuoka et al., *"Post-CHS Project"*, Plasma Physics Reports **23** No. 7 (1997), pp. 588

[26] G. H. Neilson et al., *"Physics issues in the design of High-beta, low-aspect-ratio stellarator experiments"*, Phys. Plasmas **7** No. 5 (2000) pp. 1911

[27] S. A. Henneberg et al., *"Properties of a new quasi-axisymmetric configuration"*, submitted to Nucl. Fusion

[28] M. Borchardt, *private communication*

[29] V. V. Nemov et al., *"Evaluation of $1/\nu$ neoclassical transport in stellarators"*, Phys. Plasmas **6** No. 12 (1999) pp. 4622

[30] V. V. Nemov et al., *"The ∇B drift velocity of trapped particles in stellarators"*, Phys. Plasmas **12** (2005) 112507

[31] R. H. Fowler, J. A. Rome, J, F. Lyon, *"Monte Carlo studies of transport in stellarators"* Phys. Fluids **28** (1), Jan 1985, pp. 338